STRUCTURAL CONTROL AND HEALTH MONITORING
Struct. Control Health Monit. 2006; **13**:10–26
Published online 21 December 2005 in Wiley InterScience (www.interscience.wiley.com). DOI: 10.1002/stc.145

Fluid-induced rotordynamic forces and instabilities

Christopher E. Brennen*,† and Allan J. Acosta

California Institute of Technology, Pasadena, CA 91125, U.S.A.

SUMMARY

In the late 1970s, the authors began a collaboration with our colleague Tom Caughey that helped define a new set of fluid–structure interaction phenomena in turbomachines, namely fluid-induced rotordynamic forces and instabilities. That collaboration and the 31 joint 'ABC' papers it produced epitomized Tom Caughey's genius and we reprise it here in his honor.

The design of the space shuttle main engine (SSME) pushed beyond the boundaries of many known technologies. In particular, the rotating speeds and operating conditions of the high speed liquid oxygen and liquid hydrogen turbopumps were extreme and early testing revealed a whirl instability whose magnitude exceeded expectations and allowable limits. It was suspected and later proven that fluid-induced rotordynamic effects were a contributing factor and yet very little was known of such phenomena. As one of the efforts seeking understanding, we constructed a facility to measure fluid-induced rotordynamic forces. This was subsequently used in a broad range of investigations. Initially, the effort was directed to understanding the source and parametric variations of destabilizing fluid forces. Later various components of the flow in a high speed turbopump were investigated. And finally, some ameliorative measures and their effectiveness were examined. This paper reviews this body of knowledge and the lessons learnt along the way. Copyright © 2005 John Wiley & Sons, Ltd.

KEY WORDS: rotordynamics; instabilities; turbopumps; fluid forces; fluid-structure interaction; rocket engines

1. IN MEMORIAM

In the late 1970s, the authors began a collaboration with our colleague Tom Caughey that helped define a new set of fluid–structure interaction phenomena in turbomachines, namely fluid-induced rotordynamic forces and instabilities. That collaboration and the 31 joint 'ABC' papers it produced epitomized Tom Caughey's genius and we reprise it here in his honor. Tom not only brought a rigor to our dynamic analysis and mathematical constructs but his engineering experience was invaluable in the design and fabrication of a unique experimental facility whose success has yet to be matched by any other similar research effort. He was indeed a man for all seasons. We honor not only his technical brilliance but also his humility and friendship.

*Correspondence to: C. E. Brennen, Mail Code 104-44, California Institute of Technology, Pasadena, CA 91125, U.S.A.
†E-mail: brennen@its.caltech.edu

Contract/grant sponsor: NASA George Marshall Space Flight Center; contract/grant number: NAG8-1934
Contract/grant sponsor: Advanced Rotating Machinery group of Rocketdyne

Received 30 May 2005
Revised 6 September 2005

2. PREAMBLE

The design of the space shuttle main engine (SSME) pushed beyond the boundaries of many known technologies. In particular, the rotating speeds and operating conditions of the high speed liquid oxygen and liquid hydrogen turbopumps were extreme indeed and early testing revealed a whirl instability whose magnitude exceeded expectations and allowable limits. Rotordynamic instabilities in machines rotating at nearly 40 000 rpm in cryogenic liquids are clearly very serious in any context and potentially catastrophic in rocket engines. Early on it was suspected that fluid-induced rotordynamic effects might be a contributing factor and yet very little was known of such phenomena for it had historically been assumed that the fluid would simply damp out the whirl motions and therefore the conservative approach would be to ignore its effects. Countering that there were known destablizing effects due to the fluid in bearings and seals [1–3].

In response to this crisis, NASA, in addition to the engineering fixes [4], launched several research investigations designed to provide some long-term fundamental understanding of these fluid-induced rotordynamic effects. Dara Childs, who had already done important work on the effects in hydrodynamic seals, was to expand his program at Texas A&M to research that aspect of the problem. At Caltech, the three of us were charged with examining the effects that might result from the main flow through the impeller itself. Given the complex nature of these unsteady, turbulent, cavitating flows it was clear that a fundamental experimental investigation was essential and it was this effort that formed the core of the body of work we describe below.

Several of the key features of the early observations of the problem in the turbopumps deserve mention. First the observed rotor instability frequencies were significantly lower than anticipated, thus limiting the operating envelope. Second, though the turbomachine could be accelerated through the first (and perhaps second or third) rotor instability speed, it would begin to exhibit excessive vibration at the first whirl frequency when the speed approached one of the higher harmonics. Thus the instabilities were typically subsynchronous. Consequently, it would be necessary to focus attention not only on synchronous vibration but also the dynamic effects over a broad range of frequencies, ω, not only subsynchronous but also antisubsynchronous and supersynchronous. That is to say over values of ω/Ω (where Ω is the rotating speed) from negative to greater than unity. Before we outline how this was achieved we provide some background on the mathematical framework of the problem.

3. NOTATION

The forces that fluid imparts to a rotor that is performing a whirl motion within the fluid are depicted in Figure 1. The forces are decomposed into components in the directions x and y perpendicular to the axis of rotation where this co-ordinate system is fixed in the framework of the machine. The instantaneous forces are denoted by $F_x^*(t)$, $F_y^*(t)$, and the time-averaged values of these forces in the stationary frame are denoted by F_{0x}^*, F_{0y}^*. These are the steady forces commonly referred to as the radial forces or radial thrust and are summarized in Reference [5]. In this paper, we will not dwell on these forces.

The other set of forces with which this paper will be concerned are the fluid-induced rotordynamic forces that are caused by the displacement and motion of the axis of rotation. It will be assumed that this displacement is sufficiently small so that a linear perturbation model is

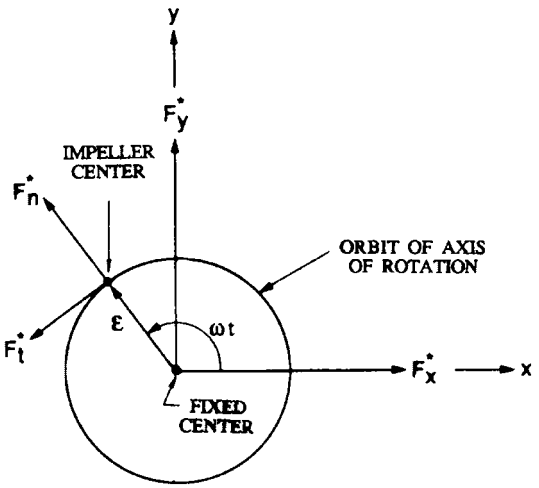

Figure 1. Schematic showing the relationship between the forces in the pump frame, F_x^*, F_y^*, the rotordynamic forces, F_n^*, F_t^*, the impeller centre, and the whirl orbit.

accurate. Then

$$\begin{Bmatrix} F_x^*(t) \\ F_y^*(t) \end{Bmatrix} = \begin{Bmatrix} F_{0x}^* \\ F_{0y}^* \end{Bmatrix} + [A^*] \begin{Bmatrix} x(t) \\ y(t) \end{Bmatrix} \tag{1}$$

where the displacement is given by $x(t)$ and $y(t)$, and $[A^*]$ is known as the 'rotordynamic force matrix,' which, in the linear model, would be independent of time, t. In virtually all cases that we shall be describing here, the displacements are sinusoidal. The 'whirl' frequency of these motions will be denoted by ω (rad/s). Then, in general, the matrix $[A^*]$ will not only be a function of the turbomachine geometry and operating condition, but also of the whirl frequency, ω.

The forces will be presented here in non-dimensional form (denoted by the same symbols without the asterisk) by dividing the forces by $\rho\pi\Omega^2 R^3 L$, where ρ is the fluid density, R is the radius of the rotor (the discharge tip radius in the case of a pump) and the length L varies with the device. For centrifugal pumps, it is appropriate to use the width of the discharge for L. With axial inducers, the axial extent of the blades is used for L. The displacements are non-dimensionalized by R. It follows that the matrix $[A]$ is non-dimensionalized by $\rho\pi\Omega^2 R^2 L$. Thus

$$\begin{Bmatrix} F_x(t) \\ F_y(t) \end{Bmatrix} = \begin{Bmatrix} F_{0x} \\ F_{0y} \end{Bmatrix} + [A] \begin{Bmatrix} x(t)/R \\ y(t)/R \end{Bmatrix} \tag{2}$$

The prototypical displacement will clearly consist of a circular whirl motion of 'eccentricity', ε, and whirl frequency, ω, so that $x(t) = \varepsilon\cos\omega t$ and $y(t) = \varepsilon\sin\omega t$. As indicated in Figure 1, an alternative notation is to define 'rotordynamic forces', F_n^* and F_t^*, that are normal and tangential to the circular whirl orbit at the instantaneous position of the centre of rotation. Note that F_n^* is defined as positive outward and F_t^* as positive in the direction of rotation, Ω. It follows that

$$F_n^* = \varepsilon(A_{xx}^* + A_{yy}^*)/2, \quad F_t^* = \varepsilon(A_{yx}^* - A_{xy}^*)/2 \tag{3}$$

and it is appropriate to define dimensionless normal and tangential forces, F_n and F_t, by dividing by $\rho\pi\Omega^2R^2L\varepsilon$. Note there are many geometries in which the rotordynamic forces should be invariant to a rotation of the x, y axes. Such will be the case only if

$$A_{xx} = A_{yy} = F_n, \quad A_{yx} = -A_{xy} = F_t \tag{4}$$

This does appear to be the case for virtually all of the experimental measurements that have been made in turbomachines. Thus it becomes convenient to display the rotordynamic forces by plotting F_n and F_t as functions of the geometry, operating condition and frequency ratio, ω/Ω. This presentation of the rotordynamic forces has a number of advantages from the perspective of physical interpretation. In many applications the normal force, F_n, is modest compared with the potential restoring forces which can be generated by the bearings and the casing. The tangential force has greater significance for the stability of the rotor system. Clearly a tangential force that is in the same direction as the whirl velocity ($F_t > 0$ for $\omega > 0$ or $F_t < 0$ for $\omega < 0$) will be rotordynamically destabilizing, and will cause a fluid-induced reduction in the critical whirl speeds of the machine. On the other hand, an F_t in the opposite direction to ω will be whirl stabilizing.

Furthermore, it is conventional among rotordynamicists to decompose the matrix $[A]$ into added mass, damping and stiffness matrices according to

$$[A]\begin{Bmatrix} x/R \\ y/R \end{Bmatrix} = -\begin{bmatrix} M & m \\ -m & M \end{bmatrix}\begin{Bmatrix} \ddot{x}/R\Omega^2 \\ \ddot{y}/R\Omega^2 \end{Bmatrix} - \begin{bmatrix} C & c \\ -c & C \end{bmatrix}\begin{Bmatrix} \dot{x}/R\Omega \\ \dot{y}/R\Omega \end{Bmatrix} - \begin{bmatrix} K & k \\ -k & K \end{bmatrix}\begin{Bmatrix} x/R \\ y/R \end{Bmatrix} \tag{5}$$

where the dot denotes differentiation with respect to time, so that the added mass matrix, $[M]$, multiplies the acceleration vector, the damping matrix, $[C]$, multiplies the velocity vector, and the stiffness matrix, $[K]$, multiplies the displacement vector. Note that the above has assumed rotational invariance of $[A]$, $[M]$, $[C]$ and $[K]$; M and m are, respectively, termed the direct and cross-coupled added mass, C and c the direct and cross-coupled damping, and K and k the direct and cross-coupled stiffness. Note also that the corresponding dimensional rotordynamic coefficients, M^*, m^*, C^*, c^*, K^*, and k^* are related to the dimensionless versions by

$$M, m = \frac{M^*, m^*}{\rho\pi R^2 L}, \quad C, c = \frac{C^*, c^*}{\rho\pi R^2 L\Omega}, \quad K, k = \frac{K^*, k^*}{\rho\pi R^2 L\Omega^2} \tag{6}$$

The representation of Equation (5) is equivalent to assuming a quadratic dependence of the elements of $[A]$ (and the forces F_n, F_t) on the whirl frequency, or frequency ratio, ω/Ω. It should be emphasized that fluid mechanical forces do not always conform to such a simple frequency dependence. An example of radical departure from the quadratic form is presented later in this paper. Nevertheless, it is of value to the rotordynamicists to fit quadratics to the plots of F_n and F_t against ω/Ω, since, from the above relations, it follows that

$$F_n = M(\omega/\Omega)^2 - c(\omega/\Omega) - K, \quad F_t = -m(\omega/\Omega)^2 - C(\omega/\Omega) + k \tag{7}$$

and, therefore, all six rotordynamic coefficients can be directly evaluated from quadratic curve fits to the graphs of F_n and F_t against ω/Ω.

Since m is often small and is frequently assumed to be negligible, the sign of the tangential force is approximately determined by the quantity $k\Omega/\omega C$. Thus rotordynamicists often seek to examine the quantity $k/C = k^*/\Omega C^*$, which is often called the 'whirl ratio' (not to be confused with the whirl frequency ratio, ω/Ω). Clearly larger values of this whirl ratio imply a larger

range of frequencies for which the tangential force is destabilizing and a greater chance of rotordynamic instability.

In this paper we will focus on the forces, but it is clear that a parallel construct is relevant to a set of rotordynamic bending moments that also determine the lines of action of the forces. For these details the reader is referred to Reference [6].

It should be recognized that each of the components of a turbomachine will manifest its own rotordynamic forces, all of which need to be included in order to complete a rotordynamic analysis of the machine. In this paper we focus on the fluid-induced effects in the turbopumps.

4. ROTOR FORCE TEST FACILITY

The key components of the experimental facility [7] built to investigate fluid-induced rotordynamic forces are shown in Figure 2. The figure shows a centrifugal pump installation though various other devices were also investigated. In all cases the rotor or impeller is directly mounted on a rotating force balance, the signals from which were routed out through a slip-ring assembly. The eccentric drive mechanism imposes a circular whirl orbit on the basic main shaft

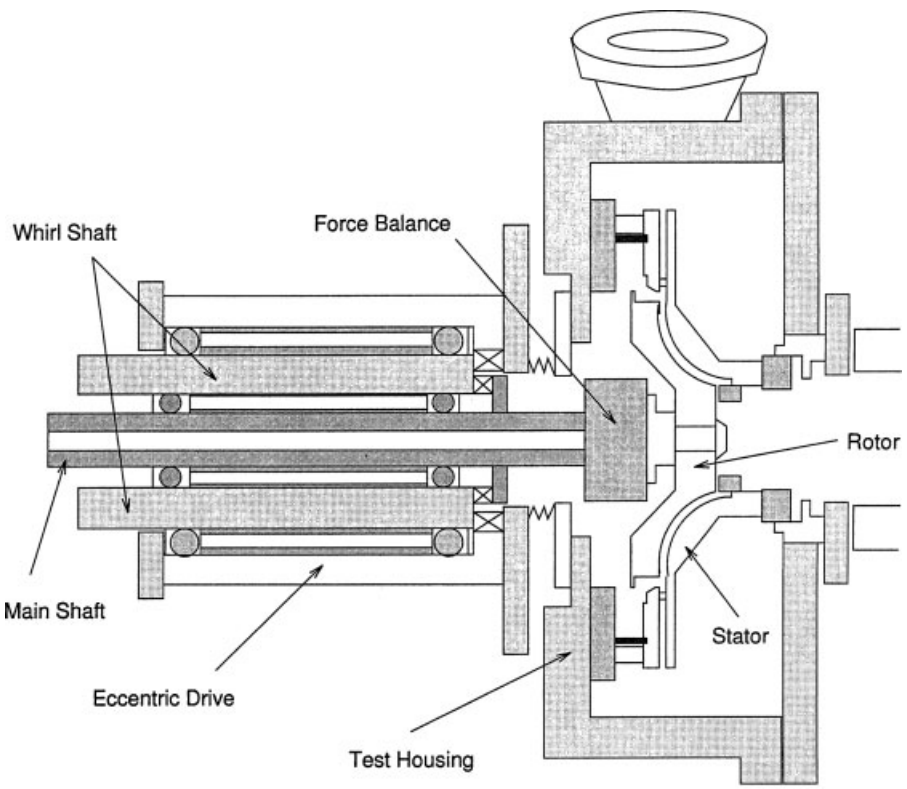

Figure 2. Schematic of the rotor force test facility.

rotation. The radius of the whirl orbit (eccentricity) could be varied; typical values used were $\varepsilon = 0.010$ in. Position sensors on both the whirl axis and the rotation axis were used to correlate the unsteady forces with the location on both orbits. Key features of the the facility were:

- Balance design. The design had to achieve adequate force measurement sensitivity yet also be stiff enough so that the critical speed of the rotor/balance system was well above the operating rotating speeds. It also had built in redundancy in case one or more of the 32 installed strain gauge bridges failed in this adverse environment.
- Feedback systems on both the main shaft motor and on the whirl motion motor had to accurately maintain the phase of these two motions. This was accomplished using a single low frequency (Ω^*) generator; two frequency multipliers then produced a signal at a frequency $J\Omega^*$ that drove the main motor with position control and a signal at a frequency $I\Omega^*$ that was used to drive the whirl motor with position control. Thus the whirl frequency ratio could be preset according to I/J.
- The motor control system was integrated with the data acquisition system in order to extract F_n and F_t. Moreover, the uncertainty could be reduced by averaging the results over many Ω^* cycles.

5. MEASUREMENTS IN CENTRIFUGAL PUMPS

Though some early data on the rotordynamic forces in a centrifugal pump were obtained by Shoji and Ohashi [8], the Caltech program added greatly to the data base. Data were obtained for many different types of impellers (centrifugal and axial, shrouded and unshrouded, with and without cavitation), for many different types of volutes and for parametric variations of the forces with pump operating point, pump cavitation and various clearances and other factors [6, 7, 9–19]. Typical data for the dimensionless normal and tangential forces, F_n and F_t, as a function of the frequency ratio, ω/Ω, are presented in Figure 3 for a conventional centrifugal pump impeller operating in a single vaneless volute. The data are typical of a wide range of different speeds, flow coefficients, and with different impellers and volutes. Perhaps the most significant feature of these results is that there exists a range of whirl frequencies for which the tangential force is whirl destabilizing. A positive F_t at negative whirl frequencies opposes the whirl motion, and is, therefore, stabilizing, and fairly strongly so since the forces can be quite large in magnitude. Similarly, at large, positive frequency ratios, the F_t is negative and is also stabilizing. However, between these two stabilizing regions, one usually finds a regime at small positive frequency ratios where F_t is positive and therefore destabilizing. This helps explain the subsynchronous whirl phenomena described earlier since, at some rotational speed above the first critical there will be a destabilizing force at the first critical frequency that may be sufficient to cause instability.

As is illustrated by Figure 3, in most instances the variation of F_n and F_t with the whirl frequency ratio, ω/Ω, can be represented quite accurately by the quadratic expressions of Equations (7) (this is not true for axial flow pumps, as will be discussed later). The rotordynamic coefficients, obtained from data like that of Figure 3 for a wide variety of speeds, flow rates, and impeller, diffuser, and volute geometries, are given in Reference [7]. We note here some of the general characteristics of these coefficients. The direct stiffness, K, is always negative because of the Bernoulli effect [5]. The cross-coupled stiffness, k, is always positive, and is directly

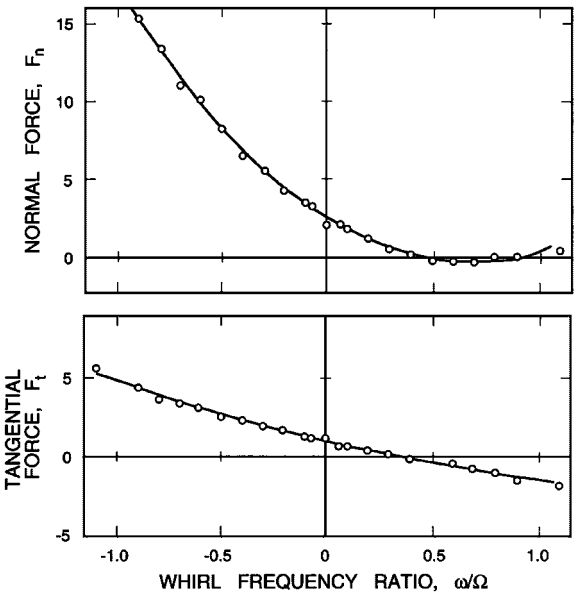

Figure 3. Typical rotordynamic forces, F_n and F_t, as a function of whirl frequency ratio, ω/Ω, for a conventional centrifugal impeller, single vaneless volute combination running at 1000 rpm and a flow coefficient of $\phi_2 = 0.092$ (from Reference [7]).

connected to the positive values of F_t at low positive whirl frequency ratios; consequently, k is a measure of the destabilizing effect of the fluid. The direct damping, C, is positive, but usually less than half of the value of the cross-coupled damping, c. The cross-coupled added mass, m, is small in comparison with the direct added mass, M, and can be neglected in many applications. Note that, since the direct added mass is converted to dimensional form by $\pi\rho R^2 L$, it follows that typical values of the added mass, M, are equivalent to the mass of about six such cylinders, or about five times the volume of liquid inside the impeller.

Note also that the value of k/C is usually a fairly accurate measure of the whirl frequency ratio corresponding to the upper bound of the destabilizing interval of whirl frequency ratios. From the data in Reference [7], the values of k/C for actual impellers with volutes and with non-zero flow, range from 0.25 to 0.40, so the range of subsynchronous speeds, for which these fluid forces are destabilizing, can be large.

We now examine the variations in the rotordynamic coefficients with the physical parameters of the flow. Note first that the non-dimensionalization satisfactorily accounts for the variation with rotational speed. Any separate effect of Reynolds number does not appear to occur within the range of speeds in these experiments. Moreover, the coefficients do not change very much with flow coefficient. Diffusers with various numbers and geometries of vanes were also tested. The presence of vanes appears to cause a slight increase in the stiffness; however, the number and type of vanes do not seem to matter. In the absence of any volute or diffuser, all of the coefficients (except m) are substantially smaller. Finally, the effect of cavitation on the rotordynamic forces in centrifugal pumps seems to be quite insignificant [12].

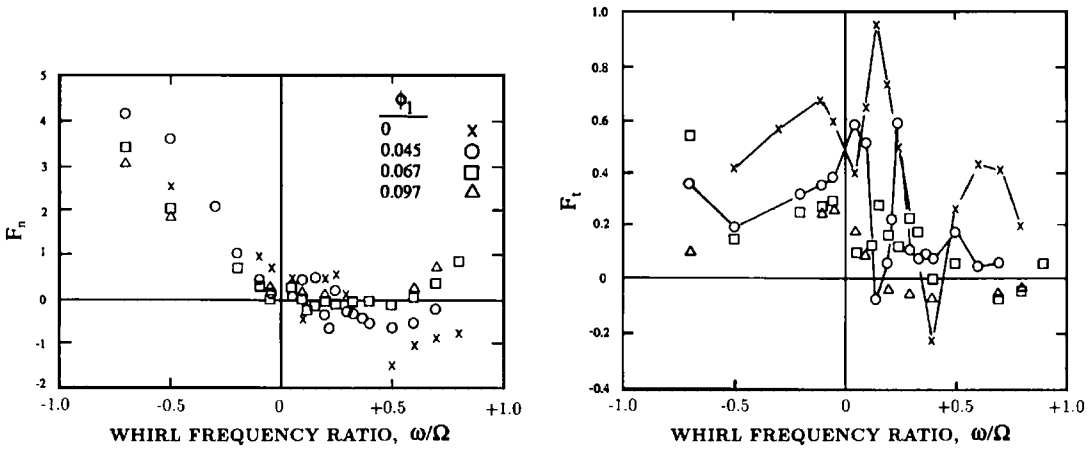

Figure 4. Rotordynamic forces for a 9° helical inducer for four different flow coefficients (from Reference [9]).

6. AXIAL FLOW INDUCERS

The rotordynamic forces in an unshrouded axial flow pump, or those caused by adding an axial inducer to a centrifugal pump, are less well understood. One of the reasons for this is that the phenomena depend on the dynamic response of the tip clearance flows, an unsteady flow that has not been studied in any detail. The experimental data that does exist [9, 11, 19] clearly show that important and qualitatively different effects are manifest by unshrouded axial flow pumps. They are exemplified by Figure 4, which presents data on F_n and F_t for a 9° helical inducer tested alone at a series of flow coefficients [9]. At the higher flow coefficients, the variation of F_n and F_t with whirl frequency ratio, ω/Ω, is similar to the centrifugal pump data. However, as the flow coefficient is decreased, somewhat pathological behaviour begins to appear in the values of F_t (and to a lesser degree F_n) at small and positive whirl frequency ratios. This culminates in extremely complicated behaviour at shut-off (zero flow) in which F_t changes sign several times for positive whirl frequency ratios, implying several separate regions of destabilizing fluid-induced rotordynamic effect. Note that the maximum values of F_t that were recorded, are large, and could well be responsible for significant vibration in an axial flow pump or inducer. Similar pathological rotordynamic effects were encountered with all the axial inducers tested, including the inducer/impeller combination represented by the high pressure LOX pump in the SSME [11]. However, the details in the variations of F_t with ω/Ω differed from one inducer to another.

Parenthetically we note that there have been a number of efforts to model the rotordynamics of impeller and inducer flows (for example, References [20, 21]); more general analyses of swirling multiphase gas/liquid flows have been attempted by d'Auria *et al.* [22].

7. CONTRIBUTIONS TO THE FLUID-INDUCED ROTORDYNAMIC FORCES

As the results for centrifugal pumps were being obtained it was recognized that contributions to the rotordynamic forces could arise not only from azimuthally non-uniform pressures in the

discharge flow acting on the impeller discharge area but also from similar non-uniform pressures acting on the exterior of the impeller front shroud as a result of the leakage flow passing between this shroud and the pump casing. Consequently, Jery *et al.* [7] also made measurements using a solid 'impeller' with the same exterior profile as the impeller of Figure 3. The leakage flow was simulated by a remote auxiliary pump which generated the same discharge to inlet pressure differences as occurred with the actual impeller. If one assumes that the solid impeller experiences the same leakage flow contributions to F_n, F_t as the actual impeller with the same profile but does not experience the main throughflow contributions, the conclusion was drawn that the leakage flow contribution to the normal force was about 70% of the total and the contribution to the tangential force was about 30% of the total. This motivated further study.

In parallel work Adkins and Brennen [23] developed a fluid mechanical model of the complicated unsteady throughflow generated when a rotating impeller whirls. The model allowed evaluation of the pressure perturbations in the impeller discharge which compared well with the experimental measurements of these perturbations. It therefore permitted evaluation of the contribution to the rotordynamic forces from these pressure perturbations and typical results for a limited range of whirl ratios are presented in Figure 5 along with experimental measurements of the total F_n, F_t under the same conditions. The conclusions are crudely consistent with the earlier remarks; the pressures in the main discharge flow contribute about one half of the rotordynamic forces. To confirm this Adkins and Brennen made pressure perturbation measurements in both the main discharge and the leakage flow. These allowed evaluation of the rotordynamic 'stiffness,' namely the rotordynamic forces at zero whirl frequency. The experiments suggested fractional contributions similar to those of Jery *et al.* [7], namely that the leakage flow contribution to the normal force was more than 70% while the contribution to the tangential force was about 40%. Adkins and Brennen also concluded that changes in the geometry of the leakage pathway could cause significant changes in these rotordynamic contributions.

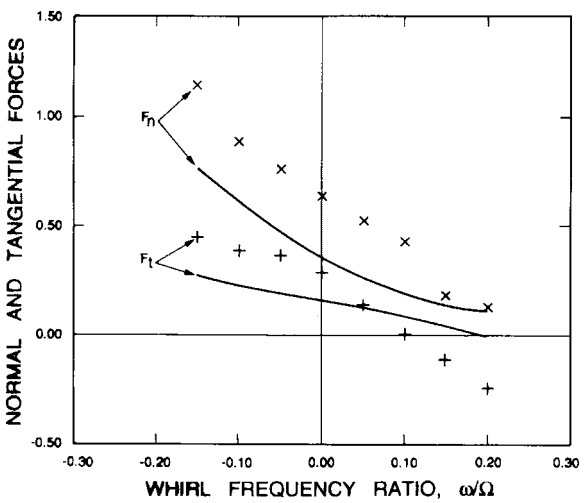

Figure 5. Comparison of the rotordynamic force contributions due to the impeller discharge pressure variations as predicted by the theory of Adkins and Brennen [23] (solid lines) with experimental measurements for a conventional centrifugal pump impeller.

Other evidence of significant leakage flow effects came from the experiments of Bolleter *et al.* [24] on a conventional centrifugal pump configuration with a much smaller leakage clearance than the experiments discussed above. These yielded rotordynamic forces with about twice the magnitude of those measured by the Caltech group.

When it became apparent that leakage flows could contribute significantly to the rotordynamics of a pump, Childs [25] adapted the bulk-flow model which he had developed for the analysis of fluid-induced forces in seals to evaluate the rotordynamic forces, F_n and F_t, due to these leakage flows. Based on lubrication theory approximations (including the assumption that the flow could be characterized by a gap-averaged velocity), this bulk flow model yielded results which had many of the correct trends. It predicted positive, rotordynamically destabilizing tangential forces over a range of positive whirl frequency ratios. However, an unusual resonance-like phenomenon was also predicted to occur at small positive whirl ratios when the inlet swirl velocity ratio (see below) exceeded about 0.5. Such resonances were not observed in the experiments.

Because of the gap-averaged velocity approximation, the model would encounter serious error when there are regions with more complex velocity profiles with, for example, flow reversals. To examine the potential for such errors, Sivo *et al.* [26] used a laser doppler velocimeter to measure the velocity profile of the leakage flow. Flow reversal close to rotor shroud was observed, in agreement with computations performed by Baskharone and Hensel [27]. The recirculation occurs at different locations in the leakage path for different conditions, and seems to diminish at higher whirl ratios. In some cases, the recirculation regions were observed around the entire impeller. They may account for the discrepancies in the model predictions. Experimental investigations of the leakage flow alone were clearly required and led us to the following experimental program.

8. LEAKAGE FLOW EXPERIMENTS

The experiments sketched in Figures 6 and 7 were installed in the rotor force test facility (Figure 2) in order to simulate impeller shroud leakage flow [14, 28] and to evaluate the rotordynamic forces caused by that flow. The gap between the rotating shroud and the stationary casing was varied by both axial and radial adjustment of the casing. Various flow rates through the gap were generated by an auxiliary pump. The rotor was driven at speeds up to 3500 rpm; a circular whirl motion with a frequency up to 1800 rpm was superimposed on that basic rotation. The amplitude of this whirl motion or eccentricity, ε, was variable and the centre of that orbit could be offset relative to the shroud. Three different leakage path geometries were tested (see Figure 7).

Both steady radial forces and rotordynamic forces were measured directly by means the rotating force balance. In addition, an array of static pressure manometer taps was located along a meridian in the leakage flow passage. By setting the rotating shroud at various fixed offsets, zero whirl frequency rotordynamic forces could be evaluated by integration of the measured pressures. The forces calculated from these pressure distributions were in good agreement with those measured directly with the force balance, thus confirming that the forces arise from the pressure variations in the leakage flow and not from the viscous shear stresses or other sources [28].

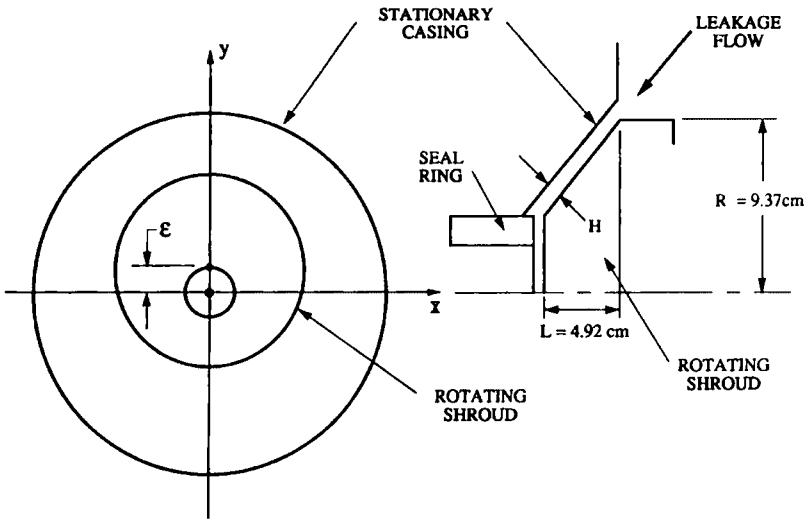

Figure 6. Schematic of the whirling shroud where ε is the eccentricity.

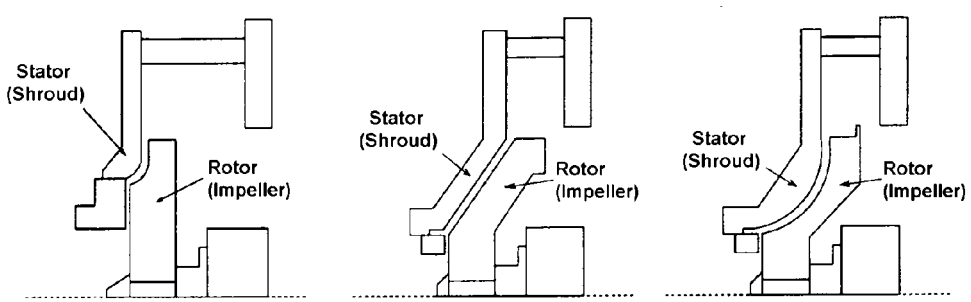

Figure 7. Three leakage path geometries tested, short contoured, conical and long contoured. From Reference [17].

Typical results from these leakage flow experiments will be presented non-dimensionally using the axial length of the leakage flow passage, L (Figure 6). In most pumps this is comparable to the pump discharge width and hence, to evaluate the significance of the results, the dimensionless data from the leakage flow tests may be directly compared with that from the impeller tests. Additional dimensionless parameters for this leakage flow data are the flow coefficient, $\varphi = Q/2\pi R^2 H\Omega$ (where Q is the leakage flow rate), the gap width ratio, H/R, the eccentricity ratio, ε/R, and the Reynolds number $\Omega R^2/\nu$ (ν is the kinematic viscosity of the liquid).

9. EXPERIMENTAL RESULTS FROM THE LEAKAGE FLOW TESTS

All the rotordynamic force data from the leakage flow experiments conformed quite closely to the quadratic form expressed in Equations (7) and therefore the discussion can focus on the

rotordynamic coefficients. Typical coefficients are shown in Figure 8 for the case of the conical geometry (a straight annular gap inclined at an angle of 45° to the axis of rotation), a rotating speed of 1000 rpm, four different leakage flow rates or flow coefficients, φ, two different clearances, H, and two eccentricities, ε. Note first that the comparison of the data for the two eccentricities confirms that the experiments lie within the linear regime of small eccentricities. Also, we note that the forces are strong functions not only of the whirl frequency ratio, ω/Ω, but also of the flow coefficient and the clearance ratio, H/R. While the dependence on flow coefficient is not simple, it would appear that the dimensionless rotordynamic forces are roughly inversely proportional to the clearance.

The effect of the flow rate or flow coefficient, φ, on the normal force coefficients (K, c, M) is clearer than its effect on the tangential force coefficients (k, C). As expected the negative K or Bernoulli effect [5] increases with increasing flow. It would also appear that the positive tangential forces at small positive whirl ratios are smallest at the highest flow rate and therefore increasing the flow is marginally stabilizing. The effect of the clearance is much larger and it seems that all the forces are roughly inversely proportional to the clearance, H. The added mass, M, could be compared with a theoretical value derived from the potential flow added mass for a

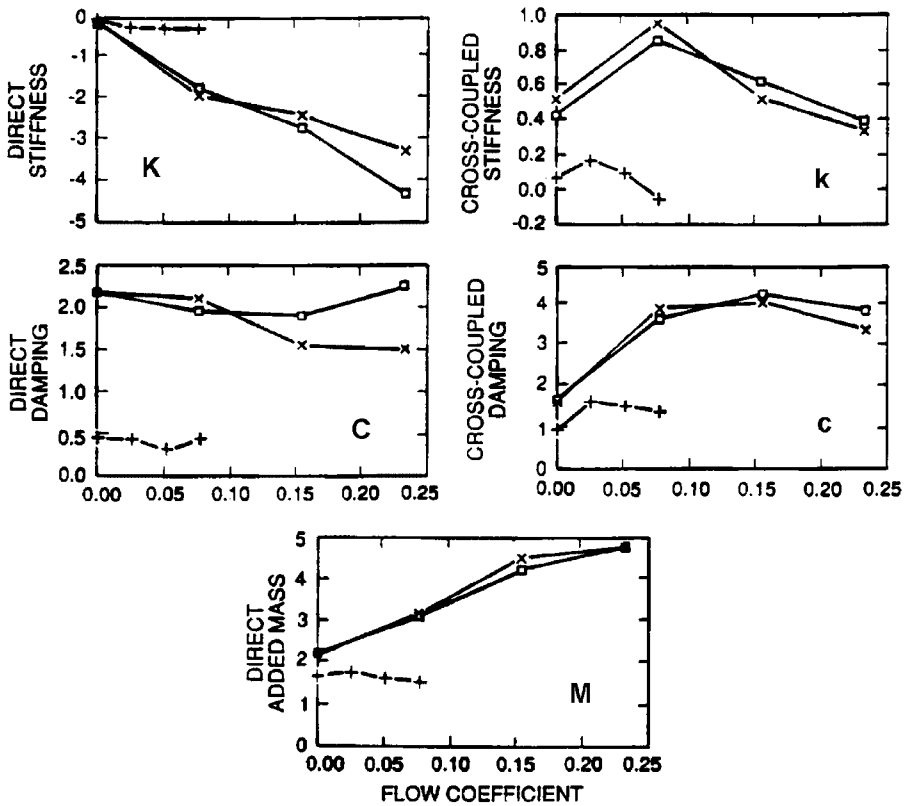

Figure 8. Dimensionless rotordynamic coefficients as functions of the flow coefficient, φ for three set of geometric parameters: $\varepsilon/R = 0.00271$, $H/R = 0.0149$ (×), $\varepsilon/R = 0.0126$, $H/R = 0.0149$ (□) and $\varepsilon/R = 0.00271$, $H/R = 0.0453$ (+). From Reference [29].

fluid-filled annulus between two circular cylinders (inner and outer radii denoted by a, b, respectively), namely $\rho\pi La^2b^2/(b^2 - a^2)$ where L is the axial length [30]. This assumes no axial velocities which could relieve the pressures caused by acceleration of the inner cylinder. If this expression is integrated over the length of the leakage annulus it leads to an added mass given by $M = 0.160R/H$ or 3.53 for $H/R = 0.0453$ and 10.74 for $H/R = 0.0149$. The fact that the actual values of M are about 40% of these may reflect the pressure relief generated by axial fluid velocity. It is however interesting to note that the above expression correctly models the inverse proportionality with H exhibited by the experimental data.

An important conclusion was the existence of an interval of forward subsynchronous whirl for which the average tangential force was destabilizing. This region decreased with increasing flow coefficient. Other factors examined experimentally were the effects of leakage path geometry, clearance, seals both at the discharge and the suction, eccentricity and Reynolds number [14, 16, 17].

10. EFFECTS OF INLET SWIRL

Guinzburg *et al.* [13, 14, 29], Uy and Brennen [16, 17] and Hsu and Brennen [18] also conducted experimental investigations of the effect on the rotordynamic forces of the inlet swirl to the leakage flow path. This was accomplished by installing guide vanes at the leakage inlet to introduce pre-rotation in the direction of shaft rotation. Figure 9 shows a typical installation designed for a swirl angle of 6° other vanes with angles of 1° and 2° were also fabricated. With this installation and assuming that the flow is parallel with the vanes, the swirl ratio, Γ (defined as the circumferential fluid velocity divided by the radial fluid velocity), depends on the flow coefficient and turning angle, α, according to $\Gamma/\varphi = H/B \tan\alpha$ where $B = 0.318$ cm is the width of the channel containing the vanes [13]. Some of the early data and analysis assumed, not unreasonably, that the flow angle would be equal to the vane angle; later this was found to be a

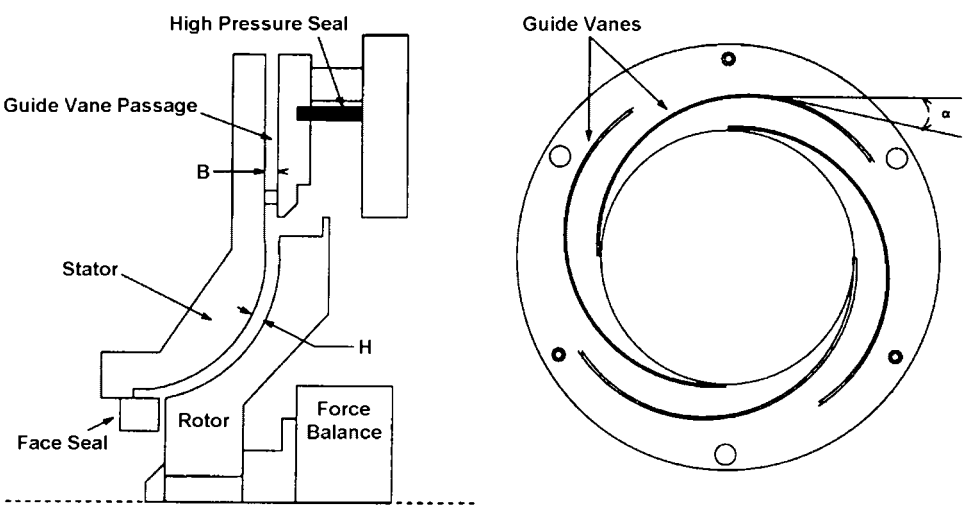

Figure 9. Inlet guide vanes; 6 degree turning angle guide vane shown.

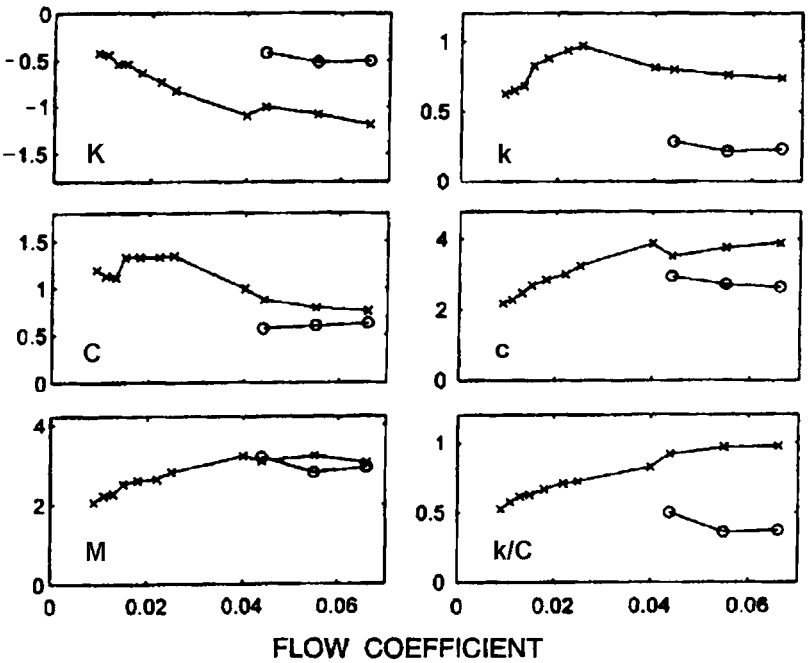

Figure 10. Rotordynamic coefficients for the contoured rotor plotted against flow coefficient, φ, for experiments with inlet swirl: $\Gamma = 0.0$ ($\circ$) and $\Gamma = 0.26$ ($\times$) [18].

serious source of error and the correct effect of inlet swirl was finally established by Hsu and Brennen [18] by direct measurement of the fluid swirl velocity and flow angle at inlet.

Typical rotordynamic data for two inlet swirl ratios, Γ, evaluated using correct, measured values of the inlet swirl, is shown in Figure 10. Examining first the normal force coefficients, M, c, and K, note that the added mass, M, does not change appreciably with inlet swirl. The magnitude of the direct stiffness, K, is larger and the magnitude of the cross-coupled damping is smaller in the absence of inlet swirl. The tangential force coefficients, C and k, both become larger with increasing swirl. In summary, the circumferential fluid velocity induced by inlet swirl affects the rotordynamic behaviour significantly, especially the whirl ratio, which defines the range of frequencies in which the tangential forces are destabilizing. Specifically, the effect of inlet swirl is destabilizing, since the magnitude of K increases and k/C increases.

11. ANTI-SWIRL RIBS AND GROOVES

We now shift attention from inlet swirl to swirl reduction by vanes installed within the leakage passage. An important finding by Sivo *et al.* [15] was that anti-swirl vanes installed on the stator within the leakage flow path could be very effective in reducing the destabilizing region of forward whirl. This is important from a practical point of view because it suggests that anti-swirl vanes in the leakage path could be used to tailor the rotordynamic behaviour of high-speed pumps.

As shown in Figure 11 the surface of the conical rotor was modified to introduce meridional ribs (0.5 cm wide and 0.16 cm high) or grooves along all or part of the length of the leakage path. Figure 12 presents typical rotordynamic force coefficients with and without these swirl braking devices [18]. Note that the magnitude of the direct stiffness K is smallest for the tests

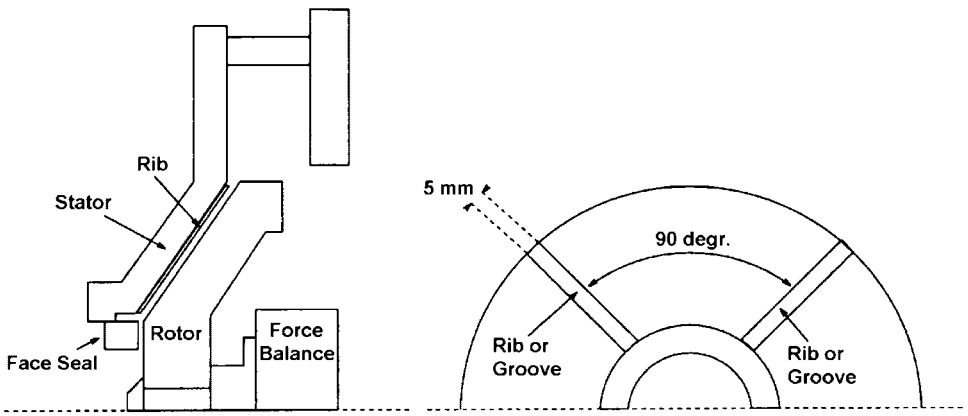

Figure 11. Sketch of the anti-swirl ribs/grooves and their location [18].

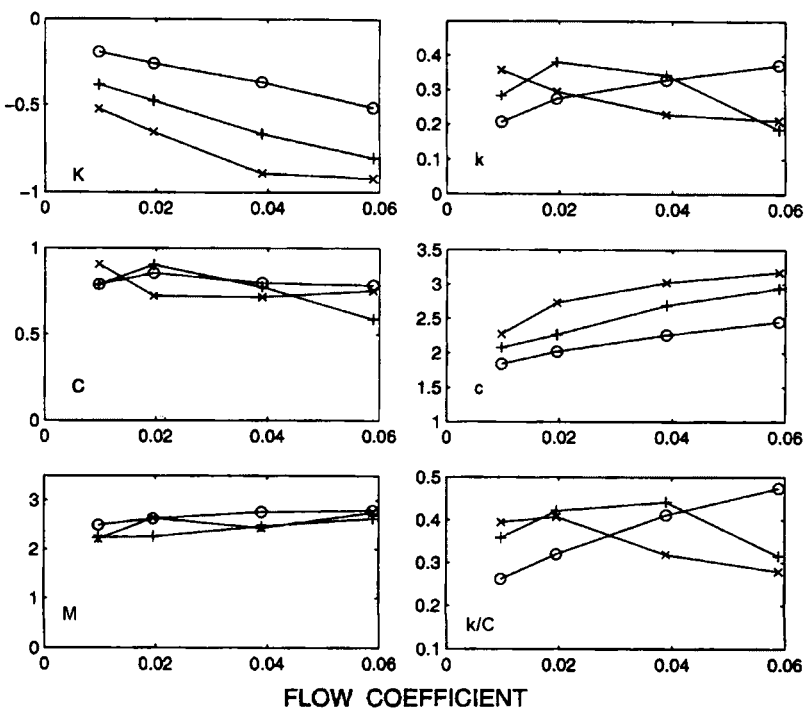

Figure 12. Comparison of rotordynamic coefficients from experiments with no anti-swirl devices (×), four full-length antiswirl ribs (◦), and four full-length antiswirl grooves (+) [18].

with no anti-swirl devices. Thus in so far as the direct stiffness is concerned, the stability is improved both with grooves and even more with anti-swirl ribs. However, the changes in the other coefficients are small though c shows some systematic change. The net result is some improvement in the destabilizing tangential force at low flow coefficient but a degradation at higher flow rates.

12. CONCLUSIONS

In summary, this project was able to identify and measure fluid-induced rotordynamic forces that can cause instability in high-speed turbomachinery. Several sources were identified in addition to the seals, namely the main flow through the impeller and auxiliary flows such as the discharge-to-suction leakage. Rotordynamic coefficients were measured for a wide range of pump designs and operating conditions. In addition, ameliorative measures such as the installation of anti-swirl vanes in the discharge-to-suction leakage path were also identified.

It is interesting to reflect on the research effort as a whole and the progression from the problem identification, to the design and fabrication of the experimental facility, the accumulation of rotordynamic coefficients, various efforts to understand the underlying fluid mechanics of these turbulent flows and, finally, the evaluation of some mitigation strategies. Our judgement would be that the most challenging task and the one least represented in the collection of publications was the design and fabrication of the experimental facility. There is such a focus on results in today's brief publications that the science and art of this design process often gets short shrift. Tom Caughey was an integral member of that design team and the success of the project owed much to his insights.

ACKNOWLEDGEMENTS

The authors know that Tom Caughey would particularly wish to acknowledge the hard work, dedication and inspiration of a generation of students at Caltech who contributed to this work including D.S. Chamieh, B. Jery, D.R. Adkins, R. Franz, N. Arndt, A. Guinzburg, J.M. Sivo, R.V. Uy, Y. Hsu, F. Zhuang, A. Bhattacharyya, M.P. Karyeaclis, W. Goda, R.S. Miskovish, F. Rahman, B.L. Bircumshaw, and many others.

We would also like to thank NASA George Marshall Space Flight Center for their encouragement and support over many years and for the support of grant number NAG8-1934 during preparation of this review. We are also grateful to the Advanced Rotating Machinery group of Rocketdyne for their support.

REFERENCES

1. Newkirk BL, Taylor HD. Shaft whipping due to oil action in journal bearing. *General Electric Review* 1925; **28**: 559–568.
2. Hori Y. A theory of oil whip. *ASME Journal of Applied Mechanics* 1959; **26**:189–198.
3. Alford JS. Protecting turbomachinery from self-excited rotor whirl. *ASME Journal of Engineering for Power* 1965; **87**:333–344.
4. Ek MC. Solution of the subsynchronous whirl problem in the high pressure hydrogen turbomachinery of the Space Shuttle Main Engine. *Proceedings of the AIAA/SAE 14th Joint Propulsion Conference*, Las Vegas, Nevada, 1978; Paper No. 78-1002.
5. Brennen C. *Hydrodynamics of Pumps*. Concepts ETI and Oxford University Press: Oxford, 1994.

6. Miskovish RS, Brennen CE. Some unsteady fluid forces measured on pump impellers. *ASME Journal of Fluids Engineering* 1992; **114**:632–637.
7. Jery B, Acosta AJ, Brennen CE, Caughey TK. Forces on centrifugal pump impellers. *Proceedings of the Second International Pump Symposium*, Houston, Texas, 1985; 21–32.
8. Shoji H, Ohashi H. Fluid forces on rotating centrifugal impeller with whirling motion. *Proceedings of the First Workshop on Rotordynamic Instability Problems in High-Performance Turbomachinery*, NASA Conference Publication 2133, College Station, TX, 1980; 317–328.
9. Arndt N, Franz R. Observations of hydrodynamic forces on several inducers including the SSME LPOTP. *Report No. E249.3*, Division of Engineering and Applied Science, California Institute of Technology, 1986.
10. Brennen CE, Acosta AJ, Caughey TK. Impeller fluid forces. *Proceedings of the NASA Advanced Earth-to-Orbit Propulsion Technology Conference*, Huntsville, AL, NASA Conference Publication 2436, 1986; 270–295.
11. Franz R, Arndt N. Measurements of hydrodynamic forces on the impeller of the HPOTP of the SSME. *Report No. E249*, California Institute of Technology, 1986.
12. Franz R, Acosta AJ, Brennen CE, Caughey TK. The rotordynamic forces on a centrifugal pump impeller in the presence of cavitation. *ASME Journal of Fluids Engineering* 1990; **112**:264–271.
13. Guinzburg A, Brennen CE, Acosta AJ, Caughey TK. The effect of inlet swirl on the rotordynamic shroud forces in a centrifugal pump. *ASME Journal of Engineering for Gas Turbines and Power* 1993; **115**:287–293.
14. Guinzburg A, Brennen CE, Acosta AJ, Caughey TK. Experimental results for the rotordynamic characteristics of leakage flows in centrifugal pumps. *ASME Journal of Fluids Engineering* 1994: **116**:110–115.
15. Sivo JM, Acosta AJ, Brennen CE, Caughey TK. The influence of swirl brakes on the rotordynamic forces generated by discharge-to-suction leakage flows in centrifugal pumps. *ASME Journal of Fluids Engineering* 1995; **117**:104–108.
16. Uy RV, Bircumshaw BL, Brennen CE. Rotordynamic forces from discharge-to-suction leakage flows in centrifugal pumps: effects of geometry. *JSME International Journal Series B* 1998; **41**(1):230–235.
17. Uy RV, Brennen CE. Experimental measurement of rotordynamic forces caused by front shroud pump leakage. *ASME Journal of Fluids Engineering* 1999; **121**:633–637.
18. Hsu Y, Brennen CE. Effect of swirl on rotordynamic forces caused by front shroud pump leakage. *ASME Journal of Fluids Engineering* 2002; **124**(4):1005–1010.
19. Bhattacharyya A, Acosta AJ, Brennen CE, Caughey TK. Rotordynamic forces in cavitating inducers. *ASME Journal of Fluids Engineering* 1997; **119**:768–774.
20. Tsujimoto Y, Acosta AJ, Brennen CE. Theoretical study of fluid forces on a centrifugal impeller rotating and whirling in a volute. *ASME Journal of Vibration, Acoustics, Stress and Reliability in Design* 1988; **110**:263–269.
21. d'Agostino L, d'Auria F, Brennen CE. A three-dimensional analysis of rotordynamic forces on whirling and cavitating helical inducers. *ASME Journal of Fluids Engineering* 1998; **120**:698–704.
22. d'Auria F, d'Agostino L, Brennen CE. Dynamic response of ducted bubbly flows to turbomachinery-induced perturbations. *ASME Journal of Fluids Engineering* 1996; **118**:595–601.
23. Adkins DR, Brennen CE. Analyses of hydrodynamic radial forces on centrifugal pump impellers. *ASME Journal Fluids Engineering* 1988; **110**(1):20–28.
24. Bolleter U, Wyss A, Welte I, Sturchler R. Measurement of hydrodynamic matrices of boiler feed pump impellers. *ASME Journal of Vibrations, Stress and Reliability in Design* 1987; **109**:144–151.
25. Childs DW. Fluid structure interaction forces at pump-impeller-shroud surfaces for rotordynamic calculations. *ASME Journal of Vibration, Acoustics, Stress and Reliability in Design* 1989; **111**:216–225.
26. Sivo J, Acosta AJ, Brennen CE, Caughey TK, Ferguson T, Lee G. Laser velocimeter measurements in the leakage annulus of a whirling centrifugal pump. *ASME Laser Anemometry-1994, Advances and Applications* 1994; **FED-191**:111–117.
27. Baskharone E, Hensel S. Flow field in the secondary, seal-containing passages of centrifugal pumps. *ASME Journal of Fluids Engineering* 1993; **115**:702–709.
28. Zhuang F. Experimental investigation of the hydrodynamic forces on the shroud of a centrifugal pump impeller. *Report No. E249.9*. Division of Engineering and Applied Science, California Institute of Technology, Pasadena, CA, 1989.
29. Guinzburg A, Brennen CE, Acosta AJ, Caughey TK. Rotordynamic forces generated by discharge-to-suction leakage flows in centrifugal pumps. *Proceedings of the Conference on Advanced Earth-to-Orbit Propulsion Technology*, NASA Conference Publication 3092, Huntsville, AL, vol. 2, 1990; 233–245.
30. Brennen C. On the flow in an annulus surrounding a whirling cylinder. *Journal of Fluid Mechanics* 1976; **75**:173–191.

